

# A paradigm system for strong correlation and charge transfer competition

James Furness (✉ [james.w.furness.1@gmail.com](mailto:james.w.furness.1@gmail.com))

Tulane University <https://orcid.org/0000-0003-3146-0977>

Ruiqi Zhang

Tulane University <https://orcid.org/0000-0002-7820-6020>

Jianwei Sun

Tulane University <https://orcid.org/0000-0002-2361-6823>

---

## Physical Sciences - Article

**Keywords:** Hydrogen Atom, Uniform Electron Gas, Electron Behavior, Electronic Structure Methods, Fractional Nuclear Charges

**Posted Date:** June 22nd, 2021

**DOI:** <https://doi.org/10.21203/rs.3.rs-297859/v1>

**License:** © ⓘ This work is licensed under a Creative Commons Attribution 4.0 International License.

[Read Full License](#)

---

1 **A paradigm system for strong correlation and charge transfer**  
2 **competition**

3 James W. Furness,<sup>\*</sup> Ruiqi Zhang, and Jianwei Sun<sup>\*†</sup>

4 *Department of Physics and Engineering Physics,*

5 *Tulane University, New Orleans, LA 70118, USA*

6 (Dated: March 4, 2021)

In chemistry and condensed matter physics the solution of simple paradigm systems, such as the hydrogen atom and the uniform electron gas, plays a critical role in understanding electron behaviors and developing electronic structure methods. The  $\text{H}_2$  molecule is a paradigm system for strong correlation with a spin-singlet ground state that localizes the two electrons onto opposite protons at dissociation. We extend  $\text{H}_2$  to a new paradigm system by using fractional nuclear charges to break the left-right nuclear symmetry, thereby enabling the competition between strong correlation and charge transfer that drives the exotic properties of many materials. This modification lays a foundation for improving practical electronic structure theories and provides an extendable playground for analyzing how the competition appears and evolves.

7 Once the governing quantum mechanical equations for a system of electrons under exter-  
 8 nal potentials have been written down the electronic structure of the system is, in principle,  
 9 determined. In practice however, almost all electron systems must be approximated to  
 10 some degree as analytical solutions seldom exist when more than one electron is present.  
 11 The paradigm systems with exact (or near exact) solutions are critical for understanding  
 12 electron behaviors, formulating concepts, and developing electronic structure methods. For  
 13 example, the exact electronic solutions of H and  $\text{H}_2^+$  are the foundations for quantum chem-  
 14 istry illustrating the concepts of atomic and molecular orbitals respectively. The uniform  
 15 electron gas is a playground for condensed matter and many-body physics, whose accurate  
 16 solution using Quantum Monte Carlo (QMC) methods<sup>1</sup> enabled construction of the local  
 17 spin density approximation (LSDA)<sup>2-4</sup> that supports most development in density functional  
 18 theory (DFT)<sup>5,6</sup>.

19 The  $\text{H}_2$  molecule is a paradigm system with a spin-singlet ground state in which the  
 20 two electrons become strongly correlated as the bond is stretched to dissociation<sup>7,8</sup>. This  
 21 is directly analogous to the strong correlations that emerge when different nuclei compete  
 22 for valence electrons, particularly in transition metal materials. In transition metal ox-  
 23 ides for example, adjacent metallic sites can compete for the valence  $d$  electrons causing  
 24  $d_i^n d_j^n \rightarrow d_i^{n-1} d_j^{n+1}$  charge fluctuations, with  $i$  and  $j$  labeling separate metallic sites. Such  
 25 charge fluctuation involves the  $d$ - $d$  on-site Coulomb interaction  $U$  that characterizes strong  
 26 correlation between the  $d$  electrons<sup>9</sup>. Transition metal oxides host another type of charge  
 27 fluctuation resulting from competition between the oxygen and transition metal ions for  
 28 the valence electrons:  $d_i^n \rightarrow d_i^{n+1} \underline{\text{O}}$ , where  $\underline{\text{O}}$  is a hole in the oxygen valence band. This  
 29 type of fluctuation characterizes the charge transfer  $\Delta$  between the metal and the anion  
 30 valence band. Using  $U$  and  $\Delta$  as input parameters, Zaanan, Sawatzky, and Allen have  
 31 been able to calculate a metal-insulator-transition phase diagram (ZSA) for transition metal  
 32 compounds<sup>10</sup>, though direct calculation of  $U$  and  $\Delta$  is challenging for most electronic struc-  
 33 ture theories. Furthermore, a recent QMC study has shown the pure 2D Hubbard model  
 34 that only includes  $U$ , a celebrated effective Hamiltonian model for studying high critical  
 35 temperature ( $T_c$ ) cuprate superconductors, is insufficient for capturing superconductivity in  
 36 the physically important parameter regime<sup>11</sup>.

37 While  $\text{H}_2$  presents a useful paradigm system for strong correlation, the symmetric nuclear  
 38 potential from the equivalent hydrogen nuclei suppresses charge transfer, as both nuclei exert

39 an equal pull on the two electrons. This left-right symmetry can be broken by replacing  
 40 one proton with a helium nucleus, thus enabling charge transfer, driving both electrons  
 41 to localize on the heavier He nucleus, and suppressing the strong correlation. This full  
 42 replacement of strong correlation by charge transfer is unfortunate, since the competition  
 43 between them drives exotic properties in many materials. It would be desirable to have  
 44 a 2-electron paradigm system that can facilitate this competition, but the above analysis  
 45 indicates that no such system can exist in nature given that all nuclei have integer charges.  
 46 Here, we fill this role by extending  $H_2$  to a new paradigm system in which the competition  
 47 between strong correlation and charge transfer can be tuned continuously.

48 To engineer such a system we create an asymmetric nuclear potential by replacing the  
 49 hydrogen nuclei with fictitious fractional nuclear charges,  $Z_A$  and  $Z_B$ . This enables charge  
 50 transfer as  $Z_A/Z_B$  moves away from 1 without completely suppressing strong correlation.  
 51 Much like the uniform electron gas that fertilized enormous concepts in condensed matter  
 52 physics, it is of no importance that the proposed system is fictional, since the physics it  
 53 captures remain deeply relevant to real correlated materials. To make the two-electron  
 54 system charge neutral we choose  $Z_A + Z_B = 2$  and, without loss of generality, we require  
 55  $Z_A \leq Z_B$  for simplicity. We term this as “ $H_2^{\text{FNC}}$ ”, where FNC stands for “fractional nuclear  
 56 charge”. Related systems were investigated by Cohen and Mori-Sánchez in the context of  
 57 the DFT derivative discontinuity and delocalization error in Ref 12.

58 For the  $H_2^{\text{FNC}}$  paradigm system to be of any use it requires an exact solution. Hartree–Fock  
 59 (HF) theory is exact for single electron systems such as H and  $H_2^+$  (up to the chosen basis  
 60 set), but it is insufficient for systems of multiple electrons. It is difficult in general to obtain  
 61 exact solutions for multi-electron systems, normally requiring exponentially scaling methods  
 62 such as full configuration-interaction (FCI) or QMC. Fortunately, the two electron systems  
 63 of interest here are small enough such that coupled-cluster at the singles-doubles (CCSD)  
 64 level is equivalent to FCI, considering all possible excitations. We note however, that CCSD  
 65 is not generally reliable for strongly correlated systems with more than two electrons. It  
 66 is precisely this easy availability of exact solutions that make paradigm systems valuable  
 67 assets for accessing the underlying physics of complex problems.

68 There are two possible electronic configurations for the  $H_2^{\text{FNC}}$  system when the fractional  
 69 nuclei are infinitely separated: a single occupation (SO) solution,  $|\Psi_{\text{SO}}\rangle$ , with one electron  
 70 on each nucleus characterizing strong correlation, and a double occupation (DO) solution,

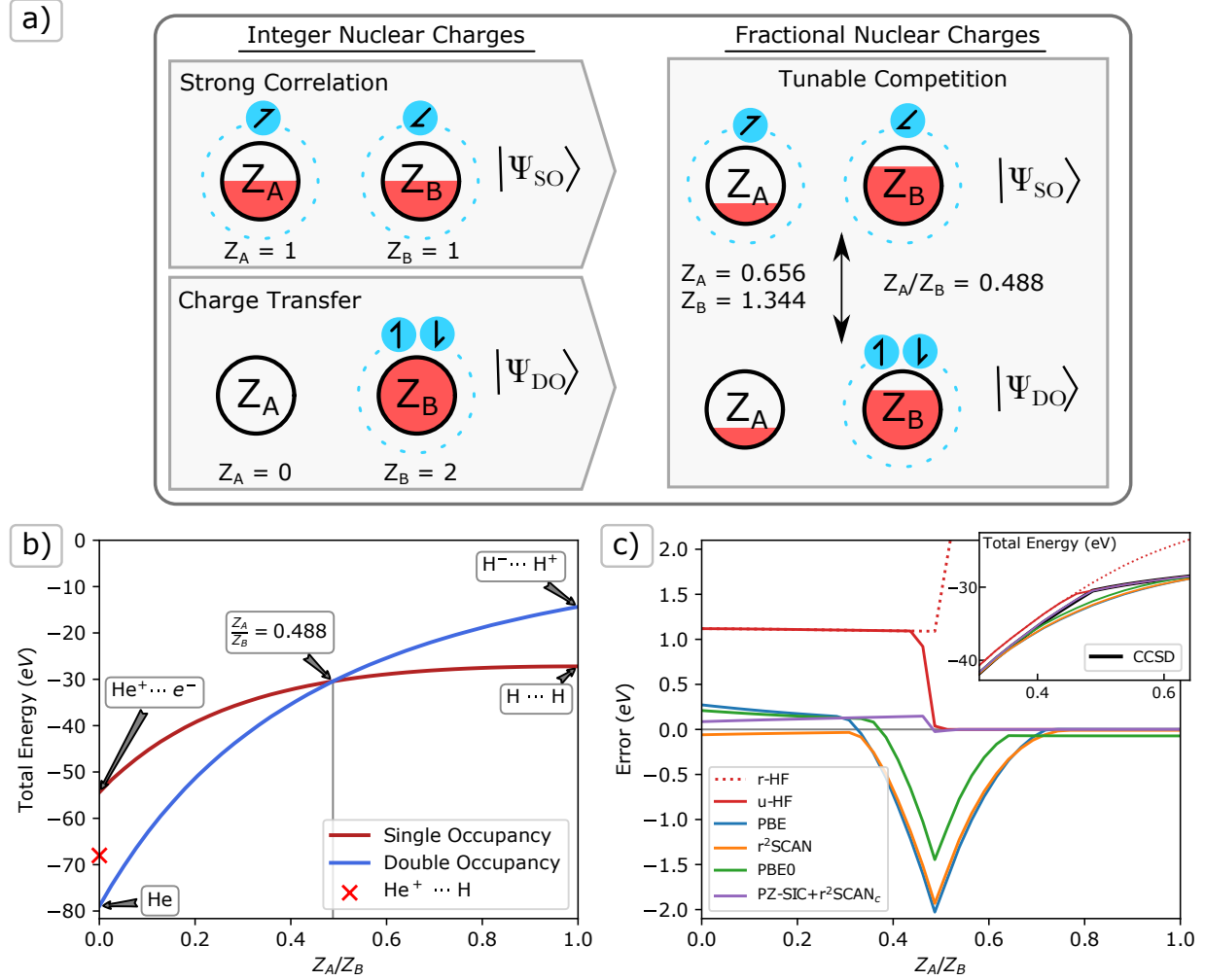


FIG. 1. **Competition between charge transfer and strong correlation illustrated by  $\text{H}_2^{\text{FNC}}$  at infinite separation.** (a) A schematic plot of the single occupancy (SO)  $|\Psi_{\text{SO}}\rangle$ , and double occupancy (DO)  $|\Psi_{\text{DO}}\rangle$  configurations in the spin-singlet state for integer and fractional nuclear charges. The nuclear charges  $Z_A$  and  $Z_B$  are constrained such that  $Z_A + Z_B = 2$  with fractional charge represented by the red area within a circle of area 2. The blue discs represent electrons with spins labeled as arrows, where tilted arrows denote spin up-down degeneracy. (b) Exact total energies for SO and DO configurations as a function of the nuclear charge ratio,  $Z_A/Z_B$ . Within annotations, “...” denotes infinite separation. (c) The errors in ground state energy calculated by HF and DFT approximations. Spin symmetry breaking (u-, solid lines) and conserving (r-, dotted lines) ground states are given for HF, while all DFT calculations are spin symmetry breaking. The corresponding total ground state energies are presented in the inset.

71  $|\Psi_{\text{DO}}\rangle$ , with both electrons on the more charged  $Z_B$  nucleus characterizing charge transfer.  
 72 Depending on the ratio  $Z_A/Z_B$ , the ground state is either the  $|\Psi_{\text{SO}}\rangle$  or  $|\Psi_{\text{DO}}\rangle$ , or the con-  
 73 figurations can become degenerate. This is summarized in Figure 1 a), while Figure 1 b)  
 74 shows how the energy of the two configurations changes across the range of  $0 \leq Z_A/Z_B \leq 1$ ,  
 75 resulting in a discontinuous ground state. At  $Z_A/Z_B = 1$ , the ground state  $|\Psi_{\text{SO}}\rangle$  is com-  
 76 prised of separated neutral hydrogen atoms, while  $|\Psi_{\text{DO}}\rangle$ , a  $\text{H}^-$  ion and a proton, is higher  
 77 in energy by about 12 eV. At  $Z_A/Z_B = 0$ ,  $Z_B$  becomes a Helium nucleus and  $Z_A$  disappears  
 78 so the converse is true:  $|\Psi_{\text{DO}}\rangle$ , a lone neutral helium atom, is favored over  $|\Psi_{\text{SO}}\rangle$ , a  $\text{He}^+$  ion  
 79 and a free electron. This is similar to the dissociation behavior of  $\text{HHe}^+$ . Allowing fractional  
 80 nuclear charges forms a continuum between these limits with the energy of each configura-  
 81 tion varying smoothly as the strong correlation of  $|\Psi_{\text{SO}}\rangle$  competes with the charge transfer  
 82 of  $|\Psi_{\text{DO}}\rangle$ . The  $|\Psi_{\text{SO}}\rangle$  and  $|\Psi_{\text{DO}}\rangle$  configurations become degenerate at  $Z_A/Z_B \approx 0.488$ , at  
 83 which point the strong correlation and charge transfer competition is maximized.

84 The appearance of degeneracy between  $|\Psi_{\text{SO}}\rangle$  and  $|\Psi_{\text{DO}}\rangle$  has profound implications. It  
 85 is well known that neither the 1D Hubbard model nor its material realization in the infinite  
 86 1D hydrogen chain shows charge transfer physics<sup>13-15</sup>. At short inter-atomic distances the  
 87 hydrogen chain is weakly correlated and metallic, while at larger inter-atomic distances it  
 88 undergoes a phase transition to a strongly correlated insulating phase<sup>13-15</sup>. The hydrogen  
 89 chain is therefore a prototypical system illustrating the Mott-Hubbard metal insulator tran-  
 90 sition. Now, consider a hydrogen chain that has a sufficiently large inter-atomic distance  
 91 such that the electron density overlap between atomic sites is negligible. Analogous to  $\text{H}_2^{\text{FNC}}$ ,  
 92 we can allow the nuclear charge for a pair of hydrogen atoms in the chain to be fractional  
 93 under the constraint the whole system remains charge neutral. Then, following the previous  
 94 analysis, the fractional nuclear charges can be tuned to make the pair close to the SO and  
 95 DO degeneracy discussed above. Around this degeneracy a small perturbation, e.g., an elec-  
 96 tric field that enhances the potential at the more positive nucleus of the pair, can easily drive  
 97 the electron from the less positive to the more positive nuclear site. This charge transfer  
 98 capability under small perturbation emerging from the insulating hydrogen chain highlights  
 99 the rich physics brought by the fractional nuclear charge. If more fractionally charged pairs  
 100 are present then more degenerate states can be generated by tuning the fractional nuclear  
 101 charges, potentially leading to exotic properties including superconductivity, even within  
 102 this 1D model<sup>16</sup>.

103 The exact solutions established above can highlight important deficiencies in common  
 104 approximate electronic structure techniques. Here we focus on DFT, which has become a  
 105 mainstay of computational materials studies. In principle, DFT is exact for the ground state  
 106 energy and electron density through an efficient mapping of the interacting-electron prob-  
 107 lem onto an auxiliary non-interacting electron system described by a single determinant. In  
 108 practice however, DFT methods must approximate the exchange-correlation energy func-  
 109 tional that carries the many-electron effects. Paradigm systems have played critical roles  
 110 in the development of exchange-correlation approximations<sup>3,17-19</sup>, with each greatly enhanc-  
 111 ing the functional’s predictive power when smoothly incorporated with other constraints.  
 112 This role is played by the uniform electron gas for LSDA<sup>2-4</sup> and the hydrogen atom for the  
 113 strongly-constrained and appropriately-normed (SCAN) density functional and its r<sup>2</sup>SCAN  
 114 revision<sup>18,19</sup>. Hartree–Fock (HF) theory is also included here for comparison as it uses a  
 115 single determinant to directly approximate the correlated wave function and is a base upon  
 116 which many more sophisticated methods are built.

117 The exact ground state wave function of the  $\text{H}_2^{\text{FNC}}$  system must be a spin singlet con-  
 118 figuration that maintains spatial symmetry between the spin-up and spin-down electrons.  
 119 For single-determinant based methods however, it is energetically advantageous to allow  
 120 different spin electrons to have different spatial distributions. This breaks the spin sym-  
 121 metry and handles the strong correlation of the ground state wave function by suppressing  
 122 the spin fluctuation. The energetic benefit of using spin symmetry breaking can be seen  
 123 when the ground state adopts the strongly correlated SO configuration, as shown in Figure  
 124 1 (c) through the comparative errors of spin symmetry conserving “restricted” HF (r-HF)  
 125 and spin symmetry breaking “unrestricted” HF (u-HF). The error of the r-HF ground state  
 126 becomes large when strong correlation dominates in  $Z_A/Z_B \gg 0.488$  where u-HF gives es-  
 127 sentially exact ground state energies by localizing the spin-up and spin-down electrons onto  
 128 separate nuclei. Localizing the electrons makes the overall system an effective sum of two  
 129 one-electron sub-systems that are well described by a single determinant. The symmetry  
 130 broken u-HF wave function is no longer an eigenfunction of the  $\hat{s}^2$  spin operator however,  
 131 and erroneously results in non-zero spin densities. The energetic benefit of symmetry break-  
 132 ing is therefore obtained at the expense of incorrect spin densities and a spin contamination  
 133 in the single determinant solution. These pathologies are well known in studies of  $\text{H}_2$ <sup>20</sup>. Re-  
 134 cently, the symmetry broken solutions revealing the strong correlation have been interpreted

135 as “freezing” a fluctuation in the exact correlated ground state wave function<sup>8</sup>. Given this  
 136 interpretation and the improved energies for strongly correlated systems we adopt the spin  
 137 symmetry breaking strategy for DFT approximations to be discussed below.

138 We have selected four non-empirical DFT exchange-correlation functionals as examples  
 139 from different levels of the Perdew–Schmidt hierarchy<sup>21</sup>. The Perdew–Burke–Ernzerhof  
 140 (PBE) functional<sup>17</sup> is a standard at the generalized gradient approximation (GGA) level and  
 141 is the simplest semi-local functional featured, taking only the spin density and its gradient as  
 142 inputs. The meta-GGA level (the most sophisticated semi-local level) is represented by our  
 143 recent r<sup>2</sup>SCAN functional<sup>18,19</sup>, which includes the non-negative kinetic energy density as an  
 144 additional ingredient that can be used to satisfy more exact constraints. Beyond the semi-  
 145 local functionals we take the PBE0 functional<sup>17,22</sup>, which replaces 25% of the PBE exchange  
 146 with 25% of the non-local exact exchange of HF. Finally, we include the r<sup>2</sup>SCAN functional  
 147 with the Perdew–Zunger self-interaction correction (PZ-SIC+r<sup>2</sup>SCAN<sub>c</sub>)<sup>23</sup> in which the self-  
 148 interaction error is removed on an orbital-by-orbital basis, equivalent to HF+r<sup>2</sup>SCAN<sub>c</sub> in  
 149 a single orbital system such as H<sub>2</sub><sup>FNC</sup>. The self-interaction error is a result of an incom-  
 150 plete cancellation of the self-Coulomb-repulsion by the self-exchange-interaction of orbitals  
 151 in DFT approximations. When PZ-SIC is combined with a one-electron self-correlation free  
 152 functional, such as r<sup>2</sup>SCAN<sub>c</sub>, then the resulting DFT calculation is exact for one-electron  
 153 systems such as H<sub>2</sub><sup>+</sup>.

154 Figure 1 (c) shows that DFT approximations are accurate for both the DO-dominant  
 155 (small  $Z_A/Z_B$ ) and SO-dominant (large  $Z_A/Z_B$ ) states, for the latter of which the spin  
 156 symmetry breaking is important. When  $Z_A/Z_B \ll 0.488$ ,  $|\Psi_{\text{DO}}\rangle$  localizes both electrons  
 157 onto the more charged  $Z_B$  and u-HF matches r-HF yielding a total energy  $\sim 1.1$  eV too  
 158 high as the short-range dynamic correlation is missed. In contrast, DFT approximations  
 159 capture the short range dynamic correlation, delivering total energies within 0.25 eV of  
 160 the reference. Severe errors are found for the DFT approximations without self-interaction  
 161 correction when  $Z_A/Z_B$  is in the region closely surrounding the degenerate point, around  
 162  $0.3 < Z_A/Z_B < 0.7$ . Here, the self-interaction error results in a spurious charge delocaliza-  
 163 tion with one electron becoming shared across both nuclei. This leads to a ground state  
 164 configuration with incorrectly fractional electron occupation numbers, even when the two  
 165 nuclei are infinitely separated<sup>12,24,25</sup>. As a result there is an erroneously smooth connection  
 166 between the  $Z_A/Z_B \rightarrow 0$  and  $Z_A/Z_B \rightarrow 1$  limits, with no discontinuity in the ground state

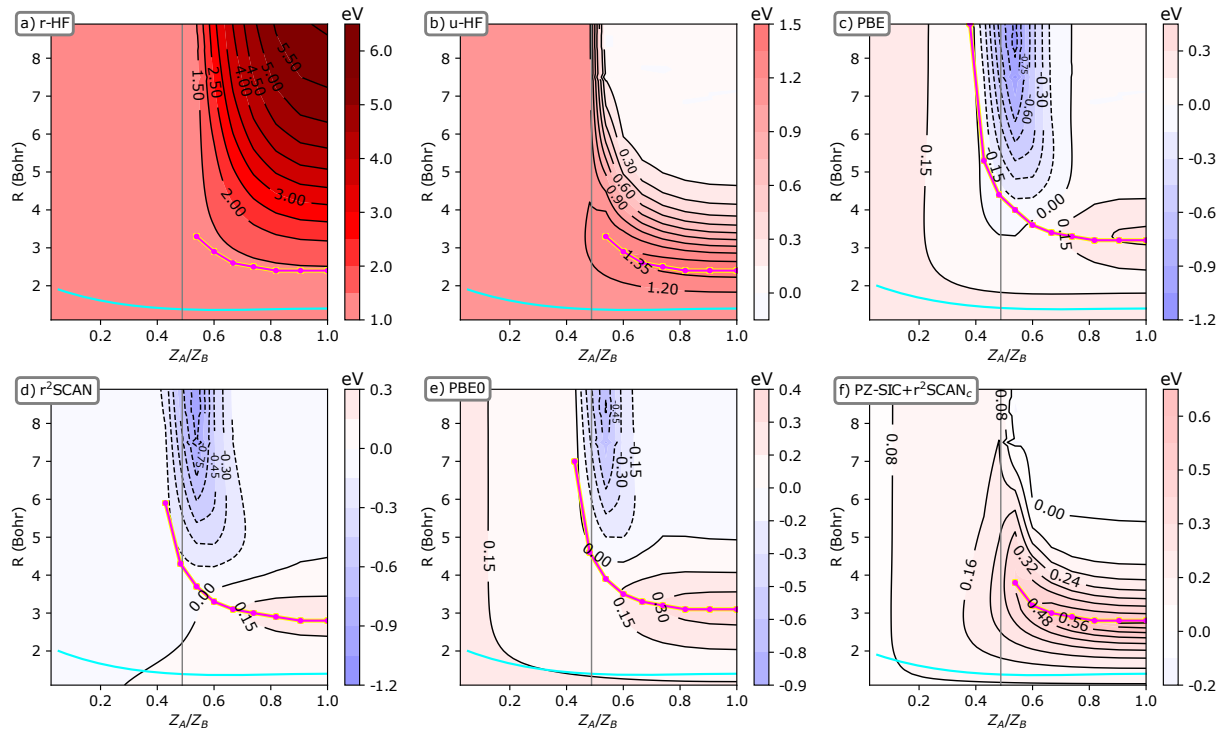


FIG. 2. The errors of different methods in  $\text{H}_2^{\text{FNC}}$  ground state total energy across the asymmetric nuclear charge ratio for finite bond lengths. Error is computed from self-consistent calculations relative to basis set exact CCSD values. Spin symmetry is conserved (r-) for a), and broken (u-) for b-f). The equilibrium bonding distance as predicted by each approximate method are highlighted with a cyan line, and the  $Z_A/Z_B = 0.488$  degeneracy point at infinite separation is shown with a gray line. The Coulson–Fisher point at which the symmetry breaking and conserving solutions split for each approximation is shown by a magenta line by sampling points along the surface until no splitting could be found. A common color scale of +6 eV (red) to -6 eV (blue) is used for all plots.

167 energy at the  $Z_A/Z_B = 0.488$  degeneracy. The error is somewhat relieved by partial inclu-  
 168 sion of the non-local exact exchange in PBE0, while it is completely corrected by the full  
 169 non-local exact exchange effectively included in PZ-SIC+r<sup>2</sup>SCAN<sub>c</sub>. While at dissociation  
 170 this problem of spurious fractional occupation can be avoided by imposing the condition of  
 171 integer occupation on the solutions, the same is not possible at finite separations which are  
 172 more relevant to real materials.

173 We now turn to  $\text{H}_2^{\text{FNC}}$  at finite separations. Figure 2 shows the landscapes of energy

174 errors relative to exact CCSD from the methods considered as functions of the  $Z_A/Z_B$  ratio  
 175 and the bond length. The equilibrium bond length for each  $Z_A/Z_B$  is highlighted as a  
 176 cyan line. Comparing r-HF (a) and u-HF (b) reveals how strong correlation is reduced  
 177 when either bond length or  $Z_A/Z_B$  decreases. Both r-HF and u-HF perform similarly once  
 178 both electrons localize into either the bonding region when the two nuclei are around the  
 179 equilibrium and  $Z_A/Z_B > 0.488$ , or onto  $Z_B$  when  $Z_A/Z_B < 0.488$ . Under these conditions  
 180 the strong correlation caused by spin symmetry is significantly reduced, and most of the  
 181 error is the result of missing short-range dynamic correlation.

182 It is well known from studies of  $H_2$  that the symmetry conserving and symmetry breaking  
 183 solutions separate at the Coulson–Fischer point<sup>27</sup>, around 2.4 Bohr for  $H_2$ . The position of  
 184 this separation is strongly affected by the nuclear charge asymmetry, occurring at longer  
 185 bond lengths as  $Z_A/Z_B$  decreases. Below the  $Z_A/Z_B = 0.488$  degeneracy, the Coulson–  
 186 Fischer point disappears as the u-HF and r-HF solutions mostly coincide, as shown in Figure  
 187 2 (a-b). We expect that the Coulson–Fischer point stretches to the infinity bond length at  
 188 the  $Z_A/Z_B = 0.488$  degeneracy if calculations with denser  $Z_A/Z_B$  and bond length grids  
 189 can be converged. It is interesting to note that the maximum error for u-HF tracks the  
 190 Coulson–Fischer point with  $Z_A/Z_B$ .

191 Figures 2 (c)-(f) show that in general the DFT approximations are a significant improve-  
 192 ment over HF as a result of their ability to capture the short-range dynamic correlation.  
 193 Two important error patterns develop however. One is the underestimation of total energy  
 194 at the region of long bond lengths ( $> 5$  Bohr) centered around the  $Z_A/Z_B = 0.488$  where  
 195 the SO-DO degeneracy occurs at infinite separation. This error appears to have the same  
 196 origin as that at infinite separation. PZ-SIC+r<sup>2</sup>SCAN<sub>c</sub> removes the self-interaction error  
 197 and gives only negligible errors at long bond lengths for the whole range of  $Z_A/Z_B$ . Note  
 198 that unlike at infinite separation it is not possible to enforce integer occupations onto nuclei  
 199 for approximate calculations, as the electrons can delocalize across both centers freely in the  
 200 exact solution.

201 The other error pattern tracks the Coulson–Fischer point with  $Z_A/Z_B$  and is similar in  
 202 nature to the u-HF error maximum. The error is roughly proportional to the percentage  
 203 of the non-local exact exchange included in the DFT approximations, with the maximum  
 204 errors of 0.65 eV for PZ-SIC+r<sup>2</sup>SCAN<sub>c</sub> (100%), 0.4 eV for PBE0 (25%), 0.35 eV for PBE  
 205 (0%), and 0.3 eV for r<sup>2</sup>SCAN (0%). The preference for a smaller fraction of exact exchange

206 in this error pattern can be explained from the error cancellation between the exchange  
 207 and correlation approximations<sup>18</sup>, which is required for good performance for normal ma-  
 208 terials. The error pattern disappears when  $Z_A/Z_B < 0.488$  as both electrons localize on  
 209 the same nucleus. This indicates the error has a multi-center origin that is non-local and  
 210 driven by the emerging strong correlation accompanied by the Coulson–Fischer point. Be-  
 211 cause the 100% nonlocal exact exchange in PZ-SIC+r<sup>2</sup>SCAN<sub>c</sub> can not take advantage of  
 212 the error cancellation with the semilocal r<sup>2</sup>SCAN<sub>c</sub> correlation for modeling the emerging  
 213 non-local strong correlation, the error develops more strongly for PZ-SIC+r<sup>2</sup>SCAN<sub>c</sub> than  
 214 for the other DFT approximations in the longer bond length domain when  $Z_A/Z_B > 0.488$ .  
 215 Interestingly, the self-interaction error that removes the discontinuity in the ground state  
 216 energy around  $Z_A/Z_B \approx 0.488$  at infinite separation results in electron density leaking onto  
 217 the less charged  $Z_A$ , allowing the Coulson–Fischer point to persist when  $Z_A/Z_B < 0.488$ .  
 218 Given the good performance of PZ-SIC+r<sup>2</sup>SCAN<sub>c</sub> at infinite separation, this highlights the  
 219 challenging problem of delivering accuracy for both regions dictated by self-interaction er-  
 220 rors and multi-center non-local strong correlation. We therefore expect that H<sub>2</sub><sup>FNC</sup> can be  
 221 a powerful tool for developing the non-local density functionals that have been the focus of  
 222 much recent DFT development<sup>28–34</sup>.

223 It is well accepted that DFT with sophisticated exchange-correlation approximations have  
 224 better accuracy than HF, and that accuracy generally improved when climbing up the the  
 225 Perdew–Schmidt hierarchy, e.g., from PBE, to r<sup>2</sup>SCAN, and to PBE0. This is consistent  
 226 with the observation in Figure 2 that general performance is improved from HF, to PBE,  
 227 to r<sup>2</sup>SCAN, and to PBE0, shown by smaller error scales and overall smaller regions of  
 228 error. Similarly, PZ-SIC has been shown as an effective correction to DFT approximations  
 229 for correlated materials due to the removal of self-interaction errors<sup>35,36</sup>. Correcting DFT  
 230 with PZ-SIC deteriorates accuracy for normal materials however, an effect which has been  
 231 called “the paradox for PZ-SIC”<sup>37</sup>. This agrees with the increased error found around the  
 232 Coulson–Fischer point for PZ-SIC+r<sup>2</sup>SCAN<sub>c</sub> in Figure 2 (f). We shall use the performance  
 233 of DFT approximations for 3*d* valence transition metal monoxides as an illustration of such  
 234 connections.

235 Table I shows the predicted electronic band gaps and magnetic moments for four typical  
 236 3*d* binary oxide antiferromagnetic (AFM) insulators (MnO, FeO, and CoO, NiO), materials  
 237 which led to the initial understanding of strongly correlated Mott insulators through on-site

TABLE I. **Comparison of theoretically predicted band gaps and local magnetic moments for four 3d transition metal monoxides.** Experimental ionic positions and lattice constants are used, with experimental reference data from Ref.<sup>39</sup> and references therein.

Structure	Band gap (eV)				Magnetic moment ( $\mu_B$ )			
	MnO	FeO	CoO	NiO	MnO	FeO	CoO	NiO
PBE	0.91	0.00	0.00	1.03	4.33	3.46	2.43	1.37
r <sup>2</sup> SCAN	1.69	0.59	0.89	2.50	4.45	3.56	2.58	1.59
PBE0	3.66	3.06	4.30	5.25	4.53	3.66	2.68	1.68
Expt. <sup>39</sup>	3.5	2.4	2.8	4.0-4.3	4.58	4.0	3.8	1.9

238 correlation localizing electrons into  $d$  bands<sup>38</sup>. Density functional methods have typically  
 239 struggled with such materials, suffering from the self-interaction error that leads to a spu-  
 240 rious charge delocalization between the metal and oxygen ions<sup>39</sup>. The delocalization error  
 241 enhances the overlap between the  $d$  orbitals of metal ions and  $p$  orbitals of oxygen ions, and  
 242 thus destabilizes the magnetic moments of metal ions, which results in too small band gaps.  
 243 The same tendency for charge delocalization is also observed in Figure 2 for  $H_2^{FNC}$  around the  
 244  $Z_A/Z_B = 0.488$  degeneracy. Comparing the predictions in Table I with the range of errors  
 245 observed in Figure 2, we see the large region of delocalization error for PBE are reflected  
 246 in underestimated magnetic moments and qualitatively incorrect band gaps. The region  
 247 of delocalization error is smaller for r<sup>2</sup>SCAN and correspondingly the material predictions  
 248 are improved, with all materials correctly insulating though significant underestimation of  
 249 band gaps remains. The partial self-interaction error correction from the non-local exchange  
 250 admixture in PBE0 further reduces delocalization error and generally improves magnetic  
 251 moments and band gaps. Early work with PZ-SIC-corrected LSDA had predictions similar  
 252 to PBE0<sup>36</sup>.

253 Finally, we would like to highlight how the fractional nuclear charges open a new door for  
 254 understanding electron behavior and electronic structure theory. The 2-electron  $H_2^{FNC}$  sys-  
 255 tem studied here informs single orbital performance and can easily be extended to 3 or more  
 256 electrons to capture multi-orbital physics. The neutral 3-electron fractional nuclear charge  
 257 diatomic can be considered as a direct analogue of the “two center, three electron” bond-  
 258 ing in homo-nuclear  $X_2^+$  diatomic cations<sup>40</sup>. The study of the charge transfer and strong

259 correlation competition in multi-orbital systems can be conducted by allowing fractional  
 260 nuclear charges for, e.g., “ $\text{Cr}_2^{\text{FNC}}$ ”. Additionally, one could increase the number of nuclear  
 261 centers present, though the spatial arrangements become less simple. A 1D chain presents  
 262  $Z_A\text{-H}_n\text{-}Z_B$  arrangements where  $Z_A/Z_B$  is tuned such that a small perturbation drives tran-  
 263 sitions between single and double occupation ground states, reflecting charge transfer across  
 264 intermediate orbitals. Alternatively, a chain of fractionally-charged nuclear pairs can be ex-  
 265 tended to infinity,  $(Z_A - Z_B)_\infty$ , or arranged into 2 and 3 dimensional lattices, analogous to  
 266 Hubbard models. Naturally, obtaining accurate reference solutions becomes more expensive  
 267 as the number of electrons increases.

268 Despite its simplicity the 2-electron  $\text{H}_2^{\text{FNC}}$  paradigm system offers a rich window into the  
 269 competing strong correlation and charge transfer physics that drive the exotic properties of  
 270 many complex materials. We have shown how calculations of  $\text{H}_2^{\text{FNC}}$  at finite and infinite  
 271 nuclear separations highlight important deficiencies in DFT approximations. This iden-  
 272 tified two major error sources originating from self-interaction error and the multi-center  
 273 non-local correlation accompanying the Coulson–Fischer point where the spin symmetry  
 274 breaking and conserving solutions meet. None of the DFT approximations considered could  
 275 remove both error sources, even when spin symmetry breaking was applied. These errors  
 276 were connected to accuracy for transition metal monoxides, showing their importance for  
 277 predicting properties of real materials. The  $\text{H}_2^{\text{FNC}}$  presented can be easily extended to more  
 278 complex multi-orbital systems, offering a clear and practical sandbox for one of the largest  
 279 problems remaining in the physical sciences.

280

## I. ACKNOWLEDGMENTS

281 J.W.F., R.Z., and J.S. acknowledge the support of the U.S. DOE, Office of Science, Basic  
 282 Energy Sciences Grant No. DE-SC0019350 (core research). We thank John Perdew and Lin  
 283 Hou for their comments.

284

## II. AUTHOR CONTRIBUTIONS

285 J.W.F. and R.Z. performed calculations and analyzed data. J.W.F. and J.S. designed  
 286 and led the investigations, designed the computational approaches, analyzed results, and

287 wrote the manuscript. J.S. provided computational resources. All authors contributed to  
288 editing the manuscript.

### 289 **III. DATA AVAILABILITY STATEMENT**

290 Data for Figures 1 and 2 is available from the authors by request.

### 291 **IV. ADDITIONAL INFORMATION**

292 Correspondence and requests for materials should be addressed to [jfurness@tulane.edu](mailto:jfurness@tulane.edu).  
293 Reprints and permissions information is available at [www.nature.com/reprints](http://www.nature.com/reprints)

### 294 **V. METHODS**

#### 295 **A. Fractional Nuclear Charges**

296 Fractional nuclear charges are implemented under the Born–Oppenheimer approximation  
297 by assigning desired  $Z_i \in \mathbb{R}^+$  to each nucleus and evaluating the nuclear-electron attraction  
298 and nuclear repulsion integrals in the standard way. This modification is trivial for most  
299 existing electronic structure codes and is available in the standard TURBOMOLE release used  
300 for this work<sup>41,42</sup>.

#### 301 **B. Figure 1**

302 Total energies calculated using TURBOMOLE V7.4 as the sum of two independent atomic  
303 calculations with fractional nuclear charges. The d-aug-cc-pV5Z hydrogen basis functions<sup>26</sup>  
304 were used for all atomic calculations. Fractional electron occupation was determined nu-  
305 merically by adjusting the occupation fraction on each atomic fragment (fixed such that the  
306 total system contains two electrons) to minimize self-consistent total energy.

307

### C. Figure 2

308 Total energies calculated for fractional nuclei at finite separation compared to CCSD  
 309 references, all calculated using TURBOMOLE V7.4. The d-aug-cc-pVQZ hydrogen basis  
 310 functions<sup>26</sup> were used for all calculations, no basis set superposition error (BSSE) correc-  
 311 tions were applied. Coulson–Fisher points were evaluated at regular steps in  $Z_A/Z_B$  by  
 312 numerically searching for the minimum bond length  $R$  ( $\pm 0.05$  Bohr) where the spin re-  
 313 stricted and spin unrestricted total energies differed by  $> 10^{-4}$  eV. No point was recorded  
 314 if no separation was found  $< 9$  Bohr.

315

### D. Table I

316 All materials are in the  $G$ -type AFM phase. Calculations use the pseudopotential  
 317 projector-augmented wave method<sup>43</sup> as implemented in the Vienna *ab initio* simulation  
 318 package (VASP)<sup>44,45</sup>. A high-energy cutoff of 500 eV was used to truncate the plane-wave  
 319 basis set.

---

320 \* jfurness@tulane.edu

321 † jsun@tulane.edu

322 <sup>1</sup> Ceperley, D. M. & Alder, B. J. Ground state of the electron gas by a stochastic method. *Physical*  
 323 *Review Letters* **45**, 566–569 (1980).

324 <sup>2</sup> Vosko, S. H., Wilk, L. & Nusair, M. Accurate spin-dependent electron liquid correlation energies  
 325 for local spin density calculations: a critical analysis. *Canadian Journal of Physics* **58**, 1200–  
 326 1211 (1980).

327 <sup>3</sup> Perdew, J. P. & Wang, Y. Accurate and Simple Analytic Representation of the Electron-Gas  
 328 Correlation-Energy. *Physical Review B* **45**, 13244–13249 (1992).

329 <sup>4</sup> Sun, J., Perdew, J. P. & Seidl, M. Correlation energy of the uniform electron gas from an  
 330 interpolation between high- and low-density limits. *Physical Review B* **81**, 085123 (2010).

331 <sup>5</sup> Hohenberg, P. & Kohn, W. Inhomogeneous electron gas. *Physical Review* **136**, B864–B871  
 332 (1964).

- 333 <sup>6</sup> Kohn, W. & Sham, L. J. Self-consistent equations including exchange and correlation effects.  
334 *Physical Review* **140**, A1133–A1139 (1965).
- 335 <sup>7</sup> Ashcroft, N. W. & Mermin, N. D. *Solid State Physics* (Harcourt College Publishers, Orlando,  
336 1976), 1 edn.
- 337 <sup>8</sup> Perdew, J. P., Ruzsinszky, A., Sun, J., Nepal, N. K. & Kaplan, A. D. Interpretations of  
338 ground-state symmetry breaking and strong correlation in wavefunction and density functional  
339 theories. *Proceedings of the National Academy of Sciences of the United States of America* **118**,  
340 1–6 (2021).
- 341 <sup>9</sup> Hubbard, J. Electron correlations in narrow energy bands. *Proceedings of the Royal Society of*  
342 *London. Series A. Mathematical and Physical Sciences* **276**, 238–257 (1963).
- 343 <sup>10</sup> Zaanen, J., Sawatzky, G. A. & Allen, J. W. Band gaps and electronic structure of transition-  
344 metal compounds. *Physical Review Letters* **55**, 418–421 (1985).
- 345 <sup>11</sup> Qin, M. *et al.* Absence of Superconductivity in the Pure Two-Dimensional Hubbard Model.  
346 *Physical Review X* **10**, 031016 (2020).
- 347 <sup>12</sup> Cohen, A. J. & Mori-Sánchez, P. Dramatic changes in electronic structure revealed by fraction-  
348 ally charged nuclei. *Journal of Chemical Physics* **140**, 044110 (2014).
- 349 <sup>13</sup> Hachmann, J., Cardoen, W. & Chan, G. K. L. Multireference correlation in long molecules  
350 with the quadratic scaling density matrix renormalization group. *Journal of Chemical Physics*  
351 **125**, 144101 (2006).
- 352 <sup>14</sup> Stella, L., Attaccalite, C., Sorella, S. & Rubio, A. Strong electronic correlation in the hydrogen  
353 chain: A variational Monte Carlo study. *Physical Review B* **84**, 245117 (2011).
- 354 <sup>15</sup> Motta, M. *et al.* Towards the solution of the many-electron problem in real materials: Equation  
355 of state of the hydrogen chain with state-of-the-art many-body methods. *Physical Review X* **7**,  
356 031059 (2017).
- 357 <sup>16</sup> Fradkin, E., Kivelson, S. A. & Tranquada, J. M. Colloquium: Theory of intertwined orders in  
358 high temperature superconductors. *Reviews of Modern Physics* **87**, 457–482 (2015).
- 359 <sup>17</sup> Perdew, J. P., Burke, K. & Ernzerhof, M. Generalized Gradient Approximation Made Simple.  
360 *Physical Review Letters* **77**, 3865–3868 (1996).
- 361 <sup>18</sup> Sun, J., Ruzsinszky, A. & Perdew, J. P. Strongly Constrained and Appropriately Normed  
362 Semilocal Density Functional. *Physical Review Letters* **115**, 036402 (2015).

- 363 <sup>19</sup> Furness, J. W., Kaplan, A. D., Ning, J., Perdew, J. P. & Sun, J. Accurate and numerically  
364 efficient r<sup>2</sup>SCAN meta-generalized gradient approximation. *The Journal of Physical Chemistry*  
365 *Letters* **11**, 8208–8215 (2020).
- 366 <sup>20</sup> Gunnarsson, O. & Lundqvist, B. I. Exchange and correlation in atoms, molecules and solids by  
367 this spin-density-functional formalism. *Physical Review B* **13**, 4274–4298 (1976).
- 368 <sup>21</sup> Perdew, J. P. & Schmidt, K. Jacob’s ladder of density functional approximations for the  
369 exchange-correlation energy. *AIP Conference Proceedings* **577**, 1–20 (2001).
- 370 <sup>22</sup> Adamo, C. & Barone, V. Toward reliable density functional methods without adjustable pa-  
371 rameters: The PBE0 model. *The Journal of Chemical Physics* **110**, 6158–6170 (1999).
- 372 <sup>23</sup> Perdew, J. P. & Zunger, A. Self-interaction correction to density-functional approximations for  
373 many-electron systems. *Physical Review B* **23**, 5048–5079 (1981).
- 374 <sup>24</sup> Perdew, J. P., Parr, R. G., Levy, M. & Balduz, J. L. Density-functional theory for fractional  
375 particle number: Derivative discontinuities of the energy. *Physical Review Letters* **49**, 1691–1694  
376 (1982).
- 377 <sup>25</sup> Mori-Sánchez, P., Cohen, A. J. & Yang, W. Localization and delocalization errors in density  
378 functional theory and implications for band-gap prediction. *Physical Review Letters* **100**, 146401  
379 (2008).
- 380 <sup>26</sup> Woon, D. E. & Dunning, T. H. Gaussian basis sets for use in correlated molecular calculations.  
381 IV. Calculation of static electrical response properties. *The Journal of Chemical Physics* **100**,  
382 2975–2988 (1994).
- 383 <sup>27</sup> Coulson, C. A. & Fischer, I. XXXIV. Notes on the Molecular Orbital Treatment of the Hydrogen  
384 Molecule. *The London, Edinburgh, and Dublin Philosophical Magazine and Journal of Science*  
385 **40**, 386–393 (1949).
- 386 <sup>28</sup> Klüpfel, S., Klüpfel, P. & Jónsson, H. The effect of the Perdew-Zunger self-interaction correction  
387 to density functionals on the energetics of small molecules. *Journal of Chemical Physics* **137**,  
388 124102 (2012).
- 389 <sup>29</sup> Pederson, M. R., Ruzsinszky, A. & Perdew, J. P. Communication: Self-interaction correction  
390 with unitary invariance in density functional theory. *Journal of Chemical Physics* **140**, 121103  
391 (2014).
- 392 <sup>30</sup> Vydrov, O. A., Scuseria, G. E., Perdew, J. P., Ruzsinszky, A. & Csonka, G. I. Scaling down  
393 the Perdew-Zunger self-interaction correction in many-electron regions. *Journal of Chemical*

- 394 *Physics* **124**, 094108 (2006).
- 395 <sup>31</sup> Cohen, A. J., Mori-Sánchez, P. & Yang, W. Fractional charge perspective on the band gap in  
396 density-functional theory. *Physical Review B* **77**, 115123 (2008).
- 397 <sup>32</sup> Maier, T. M., Arbuznikov, A. V. & Kaupp, M. Local hybrid functionals: Theory, implemen-  
398 tation, and performance of an emerging new tool in quantum chemistry and beyond. *Wiley*  
399 *Interdisciplinary Reviews: Computational Molecular Science* e1378 (2018).
- 400 <sup>33</sup> Becke, A. D. A real-space model of nondynamical correlation. *Journal of Chemical Physics*  
401 **119**, 2972–2977 (2003).
- 402 <sup>34</sup> Zope, R. R. *et al.* A step in the direction of resolving the paradox of Perdew-Zunger self-  
403 interaction correction. *Journal of Chemical Physics* **151**, 214108 (2019).
- 404 <sup>35</sup> Strange, P., Svane, A., Temmerman, W. M., Szotek, Z. & Winter, H. Understanding the valency  
405 of rare earths from first-principles theory. *Nature* **399**, 756–758 (1999).
- 406 <sup>36</sup> Szotek, Z., Temmerman, W. M. & Winter, H. Application of the self-interaction correction to  
407 transition-metal oxides. *Physical Review B* **47**, 4029–4032 (1993).
- 408 <sup>37</sup> Perdew, J. P., Ruzsinszky, A., Sun, J. & Pederson, M. R. Chapter One - Paradox of self-  
409 interaction correction: How can anything so right be so wrong? *Advances in atomic, molecular*  
410 *and optical physics* **64**, 1–14 (2015).
- 411 <sup>38</sup> Mott, N. F. *Metal-Insulator Transitions* (Taylor and Francis, London, 1974).
- 412 <sup>39</sup> Zhang, Y. *et al.* Symmetry-breaking polymorphous descriptions for correlated materials without  
413 interelectronic U. *Physical Review B* **102**, 045112 (2020). URL [https://link.aps.org/doi/](https://link.aps.org/doi/10.1103/PhysRevB.102.045112)  
414 [10.1103/PhysRevB.102.045112](https://link.aps.org/doi/10.1103/PhysRevB.102.045112).
- 415 <sup>40</sup> Zhang, Y. & Yang, W. A challenge for density functionals: Self-interaction error increases for  
416 systems with a noninteger number of electrons. *Journal of Chemical Physics* **109**, 2604–2608  
417 (1998).
- 418 <sup>41</sup> TURBOMOLE V7.5 2020, a development of University of Karlsruhe and Forschungszentrum  
419 Karlsruhe GmbH, 1989-2007, TURBOMOLE GmbH, since 2007; available from  
420 <https://www.turbomole.org>.
- 421 <sup>42</sup> Balasubramani, S. G. *et al.* TURBOMOLE: Modular program suite for *ab initio* quantum-  
422 chemical and condensed-matter simulations. *The Journal of Chemical Physics* **152**, 184107  
423 (2020).

424 <sup>43</sup> Kresse, G. & Joubert, D. From ultrasoft pseudopotentials to the projector augmented-wave  
425 method. *Physical Review B* **59**, 1758–1775 (1999).

426 <sup>44</sup> Kresse, G. & Hafner, J. Ab initio molecular dynamics for open-shell transition metals. *Physical*  
427 *Review B* **48**, 13115–13118 (1993).

428 <sup>45</sup> Kresse, G. & Furthmüller, J. Efficient iterative schemes for ab initio total-energy calculations  
429 using a plane-wave basis set. *Physical Review B* **54**, 11169–11186 (1996).